Supramolecular organization of the human N-BAR domain in shaping the sarcolemma membrane

Bertram Daum [a], Andrea Auerswald [b], Tobias Gruber [c], Gerd Hause [d], Jochen Balbach [b,c], Werner Kühlbrandt [a,*], Annette Meister [b,*]

[a] *Department of Structural Biology, Max Planck Institute of Biophysics, Max-von-Laue Str. 3, 60438 Frankfurt am Main, Germany*
[b] *Mitteldeutsches Zentrum für Struktur und Dynamik der Proteine, ZIK HALOmem, Martin Luther University Halle-Wittenberg, 06120 Halle, Germany*
[c] *Biophysics, Institute of Physics, Betty-Heimann-Str. 7, Martin Luther University Halle-Wittenberg, 06120 Halle, Germany*
[d] *Microscopy Unit, Biocenter, Weinbergweg 22, Martin Luther University Halle-Wittenberg, 06120 Halle, Germany*

ARTICLE INFO

ABSTRACT

The 30 kDa N-BAR domain of the human Bin1 protein is essential for the generation of skeletal muscle T-tubules. By electron cryo-microscopy and electron cryo-tomography with a direct electron detector, we found that Bin1-N-BAR domains assemble into scaffolds of low long-range order that form flexible membrane tubules. The diameter of the tubules closely matches the curved shape of the N-BAR domain, which depends on the composition of the target membrane. These insights are fundamental to our understanding of T-tubule formation and function in human skeletal muscle.

© 2016 The Authors. Published by Elsevier Inc. This is an open access article under the CC BY-NC-ND license (http://creativecommons.org/licenses/by-nc-nd/4.0/).

1. Introduction

The sarcolemma, the specialized membrane system of striated muscle cells, wraps around muscle fibers and forms a tubular network around each myofibril. Within this network, transversal (T-) tubules run perpendicular to the long dimension of the muscle fiber. T-tubules couple the translation of the action potential, transmitted by the nerve, into intracellular Ca^{2+}-release and muscle contraction via a large number of voltage-gated Ca^{2+} channels. Depolarization of the sarcolemma results in calcium efflux from the sarcoplasmic reticulum, which triggers muscle contraction.

Biogenesis of T-tubules is dependent on the short skeletal muscle isoform of the peripheral membrane protein Bin1 (Butler et al., 1997; Razzaq et al., 2001), in conjunction with caveolin 3 and dysferlin (Al-Qusairi and Laporte, 2011; Kerr et al., 2013). Bin1 forms arched homodimers via its N-BAR domain, which consists of two kinked trihelical coiled-coil bundles. The positively charged concave surface of N-BAR is attracted to negatively charged lipid headgroups via electrostatic interaction (Peter et al., 2004; Casal et al., 2006) and thus induces curvature in planar membranes (Fig. 1A). The N-terminal H0 domain folds into an amphipathic helix upon contact with lipids (Löw et al., 2008), which inserts into the outer membrane leaflet, enhancing membrane curvature (Bhatia et al., 2009) (Fig. 1B). Exon-10, which is expressed in the skeletal muscle isoform of Bin1, encodes for an additional domain that has been proposed to be involved in phosphoinositide binding (Lee et al., 2002).

Interactions between a variety of BAR-domain proteins and membranes have been studied by structural and computational methods (Mim and Unger, 2012). Electron cryo-microscopy (cryoEM) and helical reconstruction suggested that endophilin and amphiphysin-1 from rat induce membrane tubulation by forming close-packed helical arrays with a right-handed twist (Mim and Unger, 2012). However, the role of human N-BAR proteins in skeletal muscle T-tubules and how the tightly controlled lipid composition of the sarcolemma (Post et al., 1988) affects tubulation has not been investigated so far.

We addressed these questions by adding the human Bin1-N-BAR domain (residues 1–241) to preformed large unilamellar vesicles (LUVs) of variable lipid composition and investigating its

---

* Corresponding authors.
E-mail addresses: werner.kuehlbrandt@biophys.mpg.de (W. Kühlbrandt), annette.meister@chemie.uni-halle.de (A. Meister).
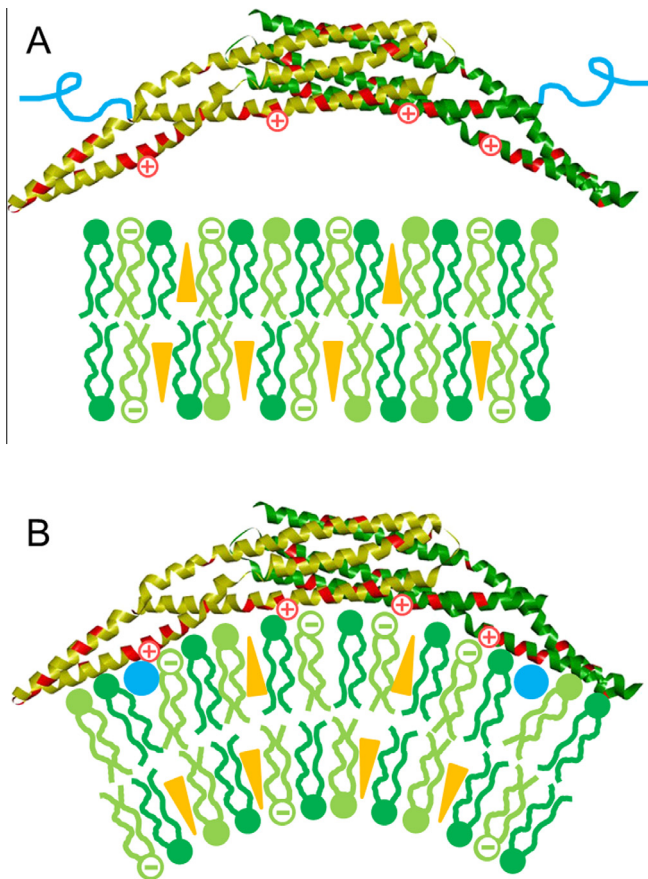
Fig. 1. Model describing membrane curvature formation by Bin1-N-BAR domain (pdb 2FIC, Casal et al., 2006). Prior to membrane binding, the amphipathic N-terminal region (blue) is disordered (A). Upon membrane binding, the N-terminal region folds into the amphipathic helix H0 (blue circle), which inserts into the outer membrane leaflet, thereby generating membrane curvature (B).

scaffolding and tube formation properties by cryoEM, electron cryo-tomography (CryoET) and sub-tomogram averaging.

2. Materials and methods

2.1. Protein purification

N-BAR (1–241) was expressed and purified as previously described (Löw et al., 2008). A modified lysis buffer (50 mM sodium phosphate, 300 mM NaCl, 20 mM imidazole, pH 8.0) was used for cell disruption and Ni affinity chromatography purification. Proteins were eluted with a gradient (0–70%) of elution buffer (50 mM sodium phosphate, 300 mM NaCl, 500 mM imidazole, pH 8.0). Thrombin digestion was performed in a dialysis tube (coff 3500 Da) and dialyzed against 20 mM Tris–Cl, 150 mM NaCl, pH 8.0. The sample was subjected to a second Ni affinity chromatography step and finally to gel filtration with 20 mM sodium phosphate, 100 mM NaCl, pH 7.4.

2.2. Large unilamellar vesicles

Reagents. The membrane lipid composition of sarcolemma and T-tubules is very similar, with a cholesterol-to-phospholipid ratio of 0.5 (Post et al., 1988; Rosemblatt et al., 1981). Commercially available Folch extract was used as a control. Vesicles were prepared from Folch extract (Folch fraction I, Sigma, St. Louis, MO, USA), SLM (sarcolemma lipid mix containing liver PC, heart PE,

brain PS, liver PI, brain PI(4,5)P$_2$, brain SM, and cholesterol) or DO-SLM (sarcolemma lipid mix containing DOPC, DOPE, DOPS, liver PI, brain PI(4,5)P$_2$, brain SM, and cholesterol) according to Post et al. (1988) and Matos et al. (1990). The lipid components of SLM and DO-SLM purchased from Avanti Polar Lipids (Alabaster, AL, USA) were bovine liver PC, bovine heart PE, bovine liver PI, porcine brain PS, porcine brain SM, porcine brain PI(4,5)P$_2$, 1,2-dioleoyl-*sn*-glycero-3-phosphocholine (DOPC), 1,2-dioleoyl-*sn*-glycero-3-phosphoethanolamine (DOPE), 1,2-dioleoyl-*sn*-glycero-3-phospho-L-serine (sodium salt) (DOPS), and ovine wool cholesterol. Lipid mixtures were prepared from lipid stock solutions in chloroform/methanol 2:1 (v/v) by combining appropriate volumes of the stock solutions according to Tables S1 and S2. The organic solvent was removed in a stream of nitrogen. Residual traces of solvent were removed under vacuum within 8 h.

Vesicle preparation. LUVs were prepared by suspending the desired amount of lipid in 20 mM aqueous phosphate buffer containing 0.1 M NaCl (pH 7.4). The lipid suspension was extruded 15 times through two 100, 200, or 400 nm diameter polycarbonate membranes. Modified SLM vesicles were prepared with half the cholesterol content (17 mol%), without cholesterol, with 1% PI (4,5)P$_2$, without PI(4,5)P$_2$, or with 5% PI instead of PIP(4,5)P$_2$.

2.3. In vitro tubulation assay

Tubulation reactions were performed with freshly extruded LUVs (25 µl, 2 mg ml^{-1}) that were incubated with protein (25 µl, 10 µM) for 2 h. For high-resolution EM imaging, LUVs (25 µl of 2 mg ml^{-1}) and protein (25 µl, 40 µM) were incubated for 30 min.

2.4. Negative stain EM

Negatively stained samples were prepared by spreading 5 µl of the dispersion onto a Cu grid coated with a Formvar-film (PLANO, Wetzlar, D). After 1 min excess liquid was blotted off with filter paper and 5 µl of 1% aqueous uranyl acetate solution were placed onto the grid and drained off after 1 min. Specimens were air-dried and examined in an EM 900 transmission electron microscope (Carl Zeiss Microscopy GmbH, Oberkochen, Germany). Micrographs were taken with a SSCCD SM-1k-120 camera (TRS, Moorenweis, Germany).

2.5. CryoEM

Samples were placed on grids coated with a holey carbon film (C-flat™, Protochips Inc., Raleigh, NC), blotted, and vitrified by plunging into liquid ethane with the grid plunger EM GP (Leica Microsystems GmbH, Wetzlar, Germany). Specimens were examined with a LIBRA 120 PLUS instrument (Carl Zeiss Microscopy GmbH, Oberkochen, Germany), operating at 120 kV. The microscope was equipped with a Gatan 626 cryotransfer system. Images were taken with a BM-2k-120 Dual-Speed on axis SSCCD-camera (TRS, Moorenweis, Germany).

2.6. CryoET

The sample was mixed 1:1 with 10 nm colloidal protein-A gold (Aurion, Wageningen, The Netherlands) and 3 µl of this solution were applied to glow-discharged 300 mesh copper Quantifoil grids (R2/2, Quantifoil, Jena, Germany). The grids were blotted for 3–5 s and rapidly plunged into liquid ethane.

Tomograms were recorded using a Polara G2 Tecnai TEM (FEI, Hillsboro, USA) or a JEM-3200 FSC (JEOL, Tokyo, Japan). Both microscopes were operated at 300 kV. The Polara was equipped with a Gatan 4 × 4 k CCD camera and a Gatan Tridiem energy filter (Gatan Inc., Pleasanton, USA). The JEM-3200FSC was equipped with
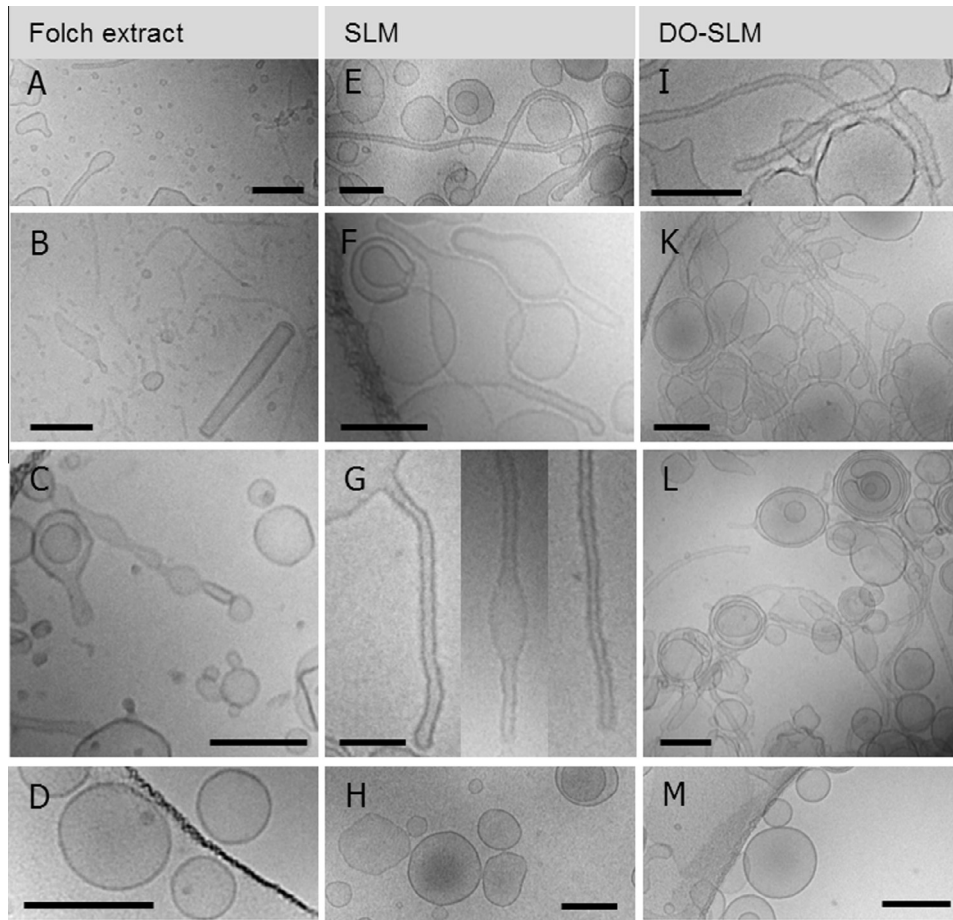
Fig. 2. *In vitro* tubulation assay. CryoEM of Folch (A–C), sarcolemma lipid mix (SLM) (E–G), and DO-SLM (I–L) vesicles after incubation with Bin1-N-BAR for 2 h. Untreated vesicles of Folch extract (D), SLM (H), and DO-SLM (M) are shown for comparison. Scale bars, 200 nm in A–F and H–M; 100 nm in (G).

an in-column energy filter and a 4×4 k K2 Summit direct electron detector (Gatan Inc., Pleasanton, USA) operating in counting mode. Zero-loss filtered images were collected using the Digital Micrograph software (Gatan Inc., Pleasanton, USA). Tilt series were collected in a range of max. $-66°$ to $+66°$ in steps of 2°, a defocus of 3–4 μm and magnifications at a final pixel size of 4.9 Å at the Polara and 3.9 at the JEM-3200 FSC. With the K2 camera, tomograms were recorded in dose-fractionation mode and a dose rate of 8–10 e^- px^{-1} s^{-1} and a total dose of ~40 e^- $Å^{-2}$. With the CCD camera data were collected at a total dose of 150 e^- $Å^{-2}$.

Dose-fractionated tilt images were aligned using the Digital Micrograph software (Gatan Inc., Pleasanton, USA). Tomograms were CTF corrected and reconstructed with the IMOD software package (Kremer et al., 1996) and contrast-enhanced using nonlinear anisotropic diffusion (NAD, Frangakis and Hegerl, 2001). The correct handedness of tomographic reconstructions was confirmed by test specimens with known chirality and orientation.

2.7. Sub-tomogram averaging

To obtain an average of a tubular segment, the center of three individual tubes of ~22 nm diameter from two tomograms was traced with linear contours in 3Dmod (IMOD, Kremer et al., 1996). To enhance low-frequency information, the tomograms were been binned twofold and filtered using nonlinear anisotropic diffusion (NAD, IMOD, Kremer et al., 1996). Along these contours, 176 points at regular distances of 10 nm were generated using

addModPts (IMOD, Kremer et al., 1996) and tubular segments cut out, aligned and averaged using PEET (Nicastro, 2009).

To obtain averages of N-BAR domains, 446 individual particles were selected from a single membrane tube in one tomogram. To aid alignment in PEET, all three Euler angles (Phi, Theta and Psi) were initially roughly predetermined. For this, the long axis of each particle was marked by two points in 3Dmod. To account for the missing wedge, particles in side-view as well as top-view orientation were selected. In Matlab (MathWorks), these points were then used to determine the rotation of each N-BAR dimer around the Euler angle Phi and to calculate the centroid of each particle. Next, the center of the flexible membrane tube was traced by open contours in 3Dmod and converted into a series of points at 1 pixel spacing using addModPts. In Matlab, a vector between each centroid and its closest neighbor within the series of points defining the tube center was determined (with knnsearch) and subsequently used to define the rotations of each particle around the Euler angles Theta and Psi.

Predefined Euler angles, as well as the centroid position of each particle were integrated into an initial motive list for PEET and an initial reference model was calculated without alignment search. Particle alignment was refined by a maximum angular search of 6° around Phi, Theta and Psi and a maximum translational search range of 3 pixels in x, y and z. In 6 iteration steps, sampling and low pass filtering was successively reduced. In the two final iterations the low pass filter was specified with a cut-off of 0.35 and a roll-off of 0.05. A cylindrical mask around the protein particle was applied to exclude the membrane and surrounding noise. To

improve the map resolution, averages were recreated using an unfiltered, CTF-corrected tomogram without binning. The alignment search was reduced to a maximum of 1.5° around all Euler angles, 2 pixels translational search in x, y and z and two iterations of refinement. As above, low pass filter values of 0.35 (cut-off) and 0.05 (roll-off) were used.

The map resolution was estimated post-alignment by Fourier shell correlation (FSC) of two particle half-sets using the program calcFSC (IMOD) and the FSC 0.5 criterion. For this, the central particle was masked using a box of x,y,z = 40,40,40 nm, excluding both neighboring particles and most of the membrane. Twofold symmetry was applied to obtain the final map of the N-BAR dimer, which was Fourier-filtered to 36 Å resolution in SPIDER (Shaikh et al., 2008).

UCSF-Chimera (Pettersen et al., 2004) was employed to display all averages and to fit the atomic structure of the BAR domain from human Bin1 (amphiphysin 2, PDB code 2FIC, Casal et al., 2006). Particles were placed back into their relative positions and orientations on the membrane surface using the EM-Package in Amira (FEI, Hillsboro, USA).

3. Results and discussion

3.1. Lipids determine the efficiency of N-BAR-mediated tubulation

Human Bin1-N-BAR (5 μM) was incubated with 1 mg/ml preformed LUVs consisting of a lipid cocktail, which closely mimics rat cardiac sarcolemma in terms of lipid head group composition and fatty acid chain length (Post et al., 1988; Matos et al., 1990; Rosemblatt et al., 1981) (Tables S1,2). This sarcolemma lipid mix (SLM) was complemented with 3% PI(4,5)P$_2$ that has been proposed to be required for binding of the exon-10 domain (Lee et al., 2002).

The Bin1-N-BAR domain was incubated with preformed SLM-LUVs (Fig. 2H) at room temperature for 2 h. CryoEM revealed that under these conditions most LUVs had converted into tubes of uniform diameter (∼22 nm; Fig. 2E–G). By contrast, incubation of Bin1-N-BAR with LUVs preformed using Folch extract yielded tubes of variable cross-section (10–70 nm; Fig. 2A, B), small ∼30 nm vesicles (Fig. 2A) or irregular "beads on a string" structures (Fig. 2C), suggesting incomplete N-BAR scaffolding. This indicates that addition of Bin1-N-BAR results in uniform tubes diameter only if the lipid mixture matches that of the sarcolemma. The tube diameter corresponds to the ∼10 nm concave curvature radius of the Bin1-N-BAR domain. The morphology of the in vitro reconstituted tubes closely resembles that of T-tubules in vivo (Ogata and Yamasaki, 1997; Hayashi et al. 1987).

In order to investigate the influence of lipid acid chain composition, we applied an artificial sarcolemma lipid mixture of 85.5 mol% pure lipids (DOPC, DOPE, DOPS, and cholesterol) together with liver PI, brain PI(4,5)P$_2$, and brain SM (14.5 mol%) (Table S1). CryoEM showed that DO-SLM vesicles converted into tubes of similar uniform diameter (∼22 nm; Fig. 2I–L) that is typical for SLM-vesicles. Mean values and standard deviation of the tube diameters are nearly identical for SLM and DO-SLM at 22.9 ± 3.4 nm and 22.6 ± 3 nm. This indicates that the lipid fatty acid distribution plays a minor role in generating curvature. However, unsaturated lipid fatty acid chains are needed to mimic the fluidity of biological membranes.

3.2. Phosphatidylinositol-4,5-bisphosphate is essential for N-BAR binding

To examine the role of individual SLM lipids in N-BAR-induced tubulation, the content of phosphatidylinositol-4,5-bisphosphate (PI(4,5)P$_2$), phosphoinositide (PI) and cholesterol was varied from
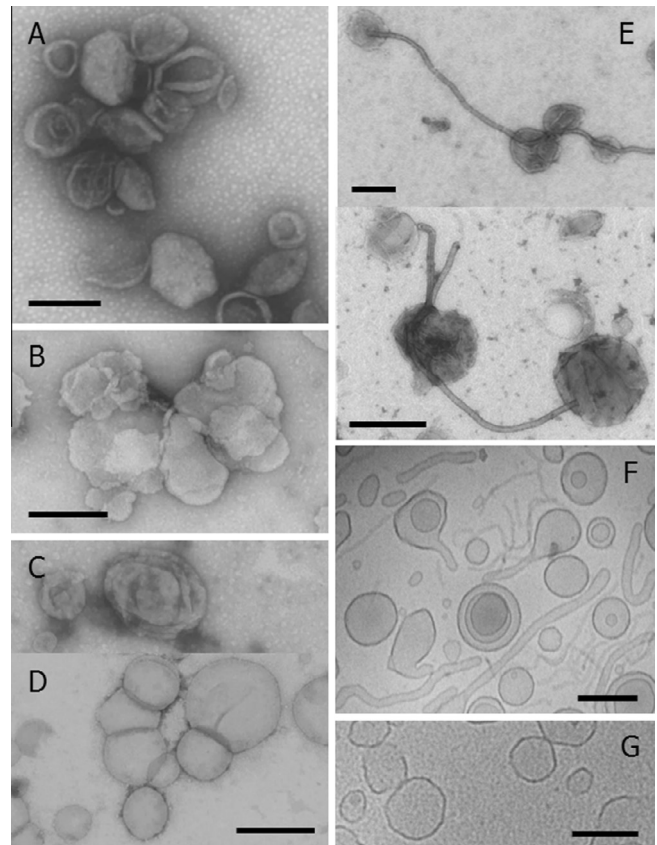

Fig. 3. Role of PI(4,5)P$_2$ and cholesterol in membrane tubulation. Negative stain EM of PI(4,5)P$_2$-free (A) and SLM vesicles containing a high level of PI (B) after incubation with Bin1-N-BAR for 2 h. PI(4,5)P$_2$-free (C) and high-PI SLM vesicles (D) without Bin1-N-BAR, and SLM vesicles after incubation with Bin1-N-BAR (E) are shown for comparison. CryoEM of cholesterol-free SLM vesicles after incubation with Bin1-N-BAR for 2 h (F). Cholesterol-free SLM vesicles without Bin1-N-BAR (G) are shown for comparison. Scale bars, 200 nm in (A–C, E–G); 500 nm in (D).

0 to 10%, 2 to 5%, or 0 to 32%, respectively. EM of negatively stained samples and cryo-EM indicated tube formation by Bin1-N-BAR only when the membranes contained PI(4,5)P$_2$ (Fig. 2E–G, I–L, Fig. 3A, E). Membrane tubulation depended on PI concentration. Tubulation was optimal at 3% PI(4,5)P$_2$ and did not increase at higher percentages. When PI(4,5)P$_2$ was replaced by PI, tubulation did not occur (Fig. 3B). The dependence of tubulation on PI(4,5)P$_2$ is surprising, as PI(4,5)P$_2$ was proposed to bind exon-10 (Lee et al., 2002), which is absent in our Bin1-N-BAR construct. Moreover, tubulation was depended on PI(4,5)P$_2$, which carries three negative charges, whereas PI, which carries a single negative charge, did not induce tubulation (Fig. 3B). This suggests that the positively charged concave surface of the N-BAR domain requires the higher charge density of PI(4,5)P$_2$ for charge compensation. These results are supported by a recent study, which demonstrated that PI(4,5)P$_2$ aids the insertion of the N-terminal amphipathic helix of Drosophila amphiphysin (Yoon et al., 2012).

As precursor of inositol triphosphate, PI(4,5)P$_2$ also regulates the muscular calcium-signaling pathway (Hilgemann et al., 2001) and hence, muscle contraction. Due to its central role in calcium signaling, N-BAR recruitment and T-tubule formation, the amount of this lipid in the sarcolemma is clearly a key factor for proper skeletal muscle function.

3.3. Cholesterol facilitates N-BAR mediated membrane tubulation

The cholesterol content of sarcolemma and T-tubule membranes has been suggested to play a major role in E-C coupling
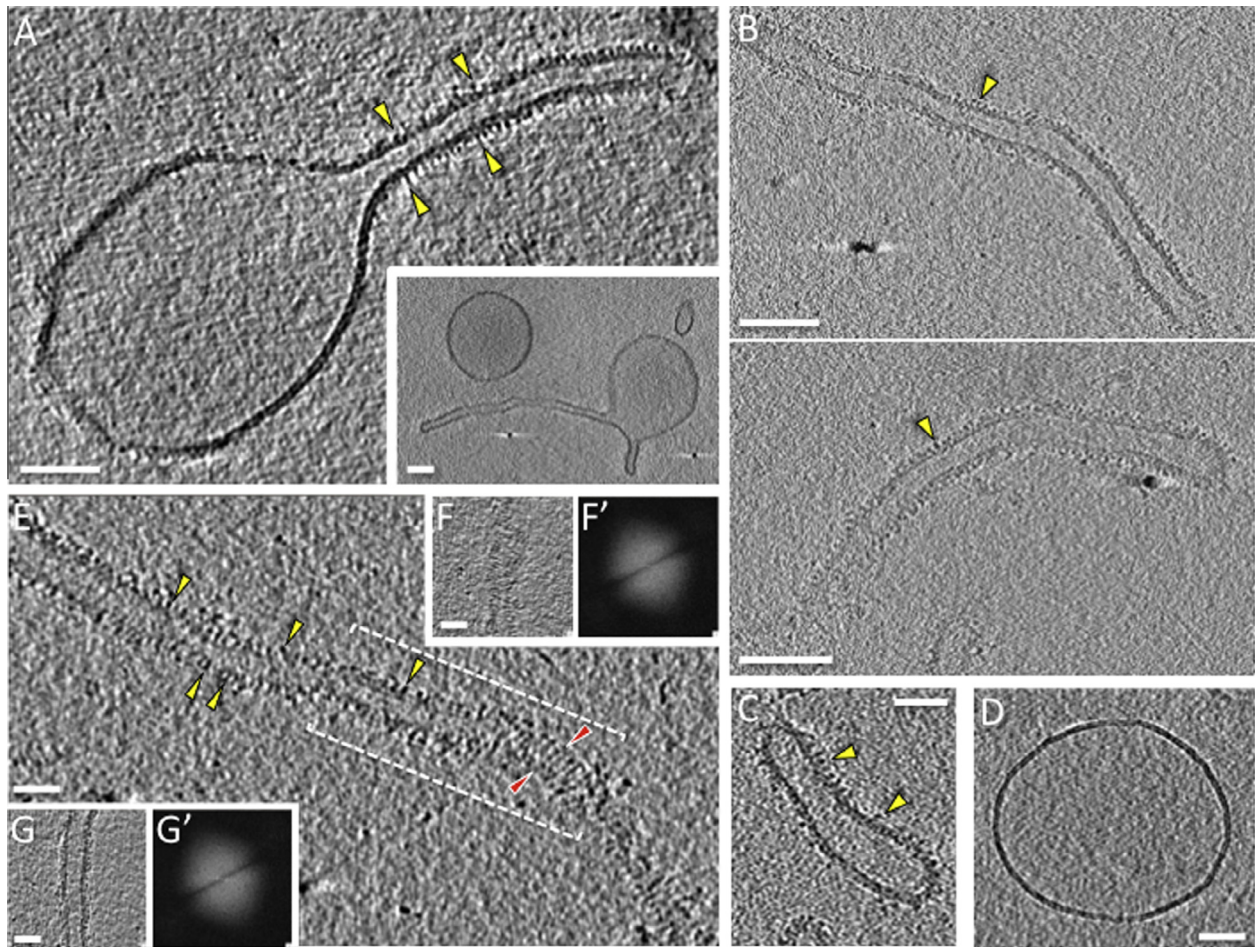
Fig. 4. Scaffolding of human N-BAR. Sections through tomograms clearly show individual 60 kDa particles forming a protein coat around tubular vesicles. Individual N-BAR domains are well resolved in side views (yellow arrowheads, A–C, E) and top views (red arrowheads, E). In spherical vesicles that show one (A) or more (inset) tubular extensions, the N-BAR coat is visible only on the tubular part. Tubes vary greatly in length (150 – several hundred nanometers) (A–C). All observed tubes are covered with N-BAR coats (A–C, E), whilst completely spherical vesicles are entirely devoid of it (D). Whereas small array-like patches seemingly occur (E, red arrowheads), the tubes are highly flexible. Dashed brackets indicate a tubular segment visualized in three dimensions in Fig. 5I. Power spectra (F′, G′) corresponding to tomographic slices through coated tubes (F, G) do not show diffraction spots, indicating a lack of long-range order. Scale bars (A–B), 50 nm; (C–G), 25 nm. All images, except inset in A were collected using the K2 camera.

by modulating membrane fluidity (Hilgemann et al., 2001). To investigate the effect of cholesterol on membrane tubulation, we prepared SLM vesicles with 50% of their endogenous cholesterol content, or without cholesterol (Fig. 3G). Incubation of Bin1-N-BAR resulted in tubules with slightly larger and less uniform cross-section (28.3 ± 4.8 nm) compared to SLM and DO-SLM. In addition, thin ~10 nm fiber-like aggregates and small ~30 nm vesicles were formed (Fig. 3F). Only membranes containing the amount of cholesterol found in the sarcolemma (32 mol%) formed native-like membrane tubes (Fig. 2G). This demonstrates the importance of the exact cholesterol content for T-tubule formation.

The comparatively low cholesterol/phospholipid ratio of the sarcolemma (Post et al., 1995) restricts the mobility of alkyl chains and decreases membrane fluidity. The distribution of cholesterol is asymmetric; it is enriched in the outer membrane leaflet, which corresponds to the inner leaflet of the T-tubule (Van der Vusse et al., 1994). With its inverted cone shape and small OH headgroup, cholesterol would support the high membrane curvature of the inner T-tubule leaflet (Fig. 1B). We suggest that a local accumulation of cholesterol promotes the invagination of T-tubules in the comparatively flat sarcolemma membrane, resulting in efficient N-BAR binding and scaffold formation.

3.4. CryoET of human N-BAR in situ

To visualize the arrangement of human Bin1-N-BAR domains on the SLM tubules, we collected electron cryo-tomograms of vitrified proteoliposomes (Fig. 4A–G). All tomograms revealed tubular vesicles of variable size and tubes of 20–30 nm cross-section. Sporadically, spherical vesicles formed one or more tubular extensions (Fig. 4A, inset), indicating the onset of N-BAR-mediated tubulation.

3.5. Scaffolding of membrane-bound Bin1-N-BAR domains

Closer inspection of the tomograms revealed a dense, striated sub-structure within the coat and individual 60 kDa Bin1-N-BAR dimers were resolved as distinct densities (Fig. 4A–C, E). Each of these particles had an elongated shape (Fig. 4E, red arrowheads) and protruded ~6 nm from the membrane plane (Fig. 4A–C, E, yellow arrowheads). On vesicles with extending tubules, the coat structure was visible only on the tubular portion (Fig. 4A) and was absent on spherical LUVs (Fig. 4D). Tubes varied greatly in length, between ~150 and several hundred nm (Fig. 4A–C).

Independent of their length, all observed tubes were covered with protein, confirming that the N-BAR coat determined their
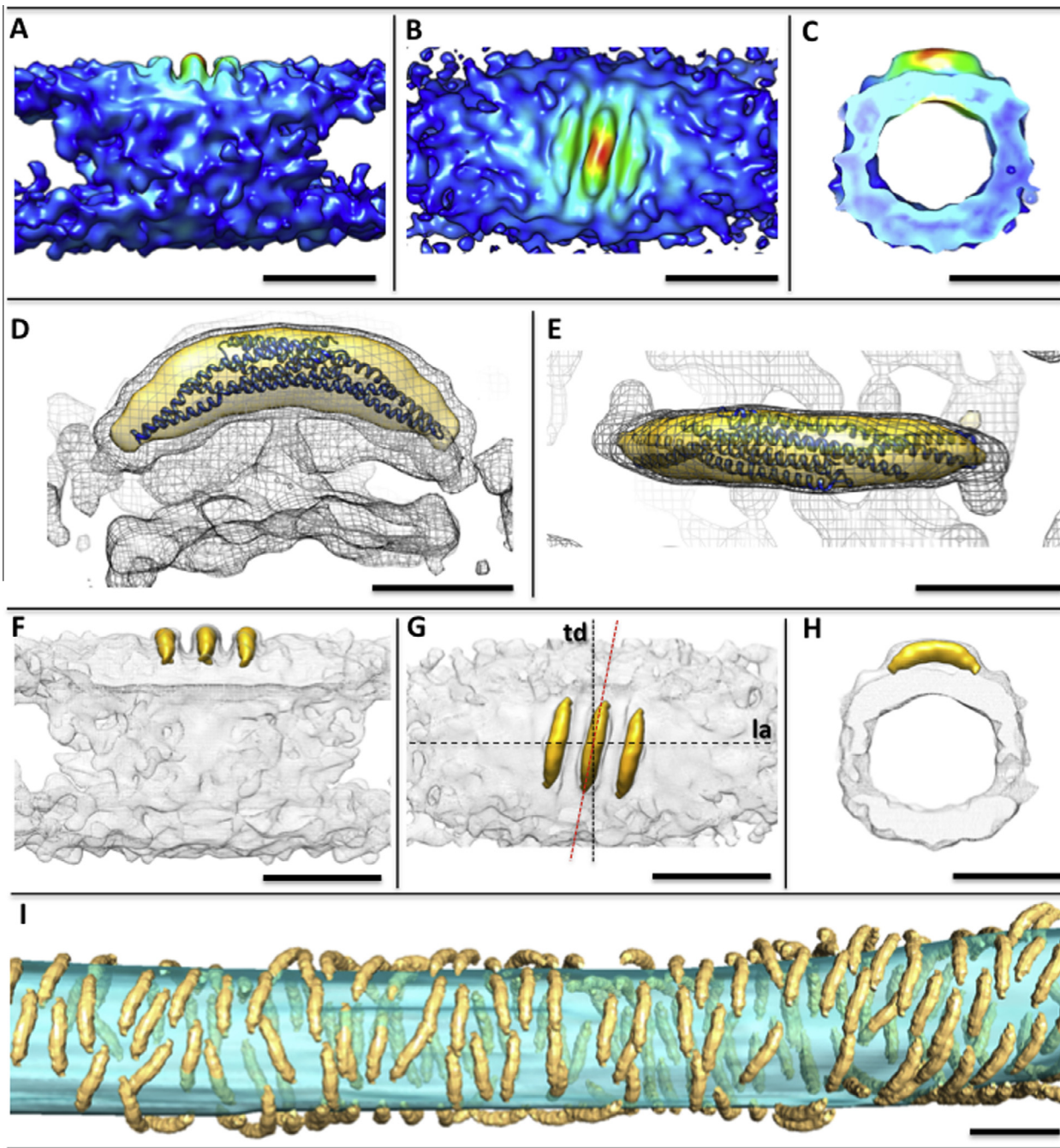
Fig. 5. Sub-tomogram averaging of the human Bin1-N-BAR domain *in situ*. Average of 446 coat particles from an NAD-filtered and twofold-binned tomogram in side-view (A), top view (B) and cross-section (C) shows the N-BAR dimer and neighboring particles as curved densities on top of a tubular membrane. Rainbow colours represent different density values (from high to low: red, yellow, green, blue). Cross-section (D) and top view (E) of the average generated without binning or NAD filter displayed at two different threshold values (transparent orange, low; grey mesh; high). The X-ray structure of the Bin1-N-BAR dimer (blue; PDB-code 2FIC, Casal et al., 2006) was fitted into the central arch-shaped density. This particle was docked into the NAD-filtered average to visualize average positions and orientations of three adjacent N-BARs in the tubular membrane more clearly (F, side-view; G, top view; H, cross-section; orange, N-BAR dimers; grey mesh, membrane; la, tube long axis; td, tube diameter; ha, helix angle). I, sub-tomogram average repositioned into the original tomogram shows negligible long-range and little short-range order within the N-BAR coat (orange, N-BAR; transparent blue, membrane). Scale bars, A–C, F–I 15 nm; D, E, 5 nm.

shape. Small repetitive patches of neighboring particles suggested limited short-range order between neighboring particles (Fig. 4E, red arrowheads), yet power spectra (Fig. 4F′, G′) calculated of tomographic slices through the tubes (Fig. 4F, G) lacked diffraction spots, indicating the absence of significant long-range order in the N-BAR coat.

3.6. Sub-tomogram averaging of N-BAR domains

To understand the three-dimensional organization of the N-BAR coat, we performed sub-tomogram averaging. Initial averaging of overlapping tubular segments resulted in maps of cylindrical membranes surrounded by a fuzzy coat, in which individual

particles were poorly resolved (Fig. S1). On account of the low order within the N-BAR coat, individual N-BARs were manually picked in twofold binned and NAD-filtered tomograms, aligned and averaged. For this, a tubular mask was applied that tightly fitted the N-BAR dimer in the center of the map. The resulting average shows a curved density that is ~12 nm long, ~4 nm wide and associated with the surface of a hollow, tubular membrane (Figs. 5A–C, S2A–C). The particle was flanked by two curved, roughly parallel but weaker densities with a center-to-center distance of ~6 nm (Fig. 5A, B). No further densities were resolved in the direction of the tube's long axis or around its circumference, suggesting high inherent intrinsic flexibility within the N-BAR coat.

To reveal the central density at greater detail, the subtomogram average was refined using the same CTF-corrected tomograms that were not previously binned or filtered. The overall map resolution of the N-BAR dimer (Figs. 5D, E; S2D–F) was 36 Å, as determined by Fourier shell correlation (FSC) (Fig. S3) and closely matched the X-ray structure of the human Bin1-N-BAR dimer (PDB 2FIC, Casal et al., 2006) (Fig. 5D, E). The density was arc-shaped, with a curvature radius of roughly 10 nm. In top view the dimer described a slight S-curve (Fig. 5E).

Superimposition of this structure with the previous (filtered, twofold binned) map revealed average positions and orientations of the central particle and its flanking densities more clearly (Fig. 5F–H). The orientation of the three N-BARs indicated that they have a tendency to arrange locally in a left-handed helix, with a helix angle of ~−6° (Fig. 5G).

To visualize the location and orientation of N-BAR dimers along a section of a reconstructed tubule, the central particle from our average was finally repositioned into the tomographic volume (Fig. 5I, Movie S1). Note that the particle density reflects the number of N-BAR dimers that could be manually selected in the tomogram prior to sub-tomogram averaging and thus may be slightly lower than in reality. However, the reconstruction clearly shows that Bin1-N-BAR assembles into a loose protein scaffold of negligible long-range order, in line with the absence of diffraction spots in the Fourier transform. Most dimers are roughly parallel with their nearest neighbors, and adopt an orientation relative to the tubular membrane that is reminiscent of a left-handed helical array. However, angles and distances between them vary by several degrees and nanometers, rendering the array highly irregular.

Previous helical real-space reconstruction of EM projections gave rise to the assumption that proteins containing N-BAR domains generate membrane tubules by assembling into highly ordered helical scaffolds (Adam et al., 2015; Suetsugu et al., 2014; Mim et al., 2012). However, this notion contradicts findings that N-BAR-covered membrane tubes are often very flexible, vary considerably in diameter and lack significant diffraction in Fourier space (Mim et al., 2012). Sub-tomogram averaging now reveals that human Bin1-N-BAR is also capable of tubulating membranes by assembling into loose scaffolds with imperfect left-handed helical symmetry, devoid of long-range order. This is consistent both with the high degree of flexibility of the tubes and the lack of diffraction. We conclude that a loose array of N-BAR domains is sufficient to tubulate the membrane. The variability of inter-domain distances and rotational offsets suggest that this scaffold forms without specific protein-protein interactions between neighboring N-BAR domains. This situation is reminiscent of ATP synthase dimer rows that define the highly curved margins of mitochondrial cristae membranes (Davies et al., 2011, 2012). Coarse-grained molecular dynamics simulations indicated that the inherent curvature of the ATP synthase dimer is sufficient to drive the assembly of multiple dimers into rows (Davies et al., 2012). We propose that a similar mechanism governs the assembly of Bin1-N-BAR domains.

The degree of order in the tubular protein coat has important functional implications. Membrane tubules formed by such soft scaffolds would be more flexible compared to a rigid, highly ordered helical array of scaffolding proteins. A high level of flexibility is particularly important for T-tubules that reside in continually contracting and expanding muscle cells.

4. Conclusions

The N-BAR domain of skeletal muscle Bin1 assembles into a loose, imperfectly ordered helical scaffold to form flexible tubules in the sarcolemma membrane. Uniform membrane tubulation by Bin1-N-BAR is sensitive to the lipid composition of the target membrane. The diameter of reconstituted T-tubules corresponds closely to the curved shape of the N-BAR domain. Our results show that the protein itself as well as the membrane lipids are important factors in determining the structure and properties of membrane tubules formed by N-BAR domains.

Additional information

We deposited the EM maps at the EM Databank (EMD-8126 and EMD-8127).

Conflict of interests

There is no conflict of interests.

Acknowledgements

Appendix A. Supplementary data

Supplementary data associated with this article can be found, in the online version, at http://dx.doi.org/10.1016/j.jsb.2016.03.017.

References

Adam, J., Basnet, N., Mizuno, N., 2015. Structural insights into the cooperative remodeling of membranes by amphiphysin/BIN1. Sci. Rep. 5, 15452.

Al-Qusairi, L., Laporte, J., 2011. T-tubule biogenesis and triad formation in skeletal muscle and implication in human diseases. Skelet. Muscle 1, 26–36.

Bhatia, V.K., Madsen, K.L., Bolinger, P.Y., Kunding, A., Hedegard, P., Gether, U., Stamou, D., 2009. Amphipathic motifs in BAR domains are essential for membrane curvature sensing. EMBO J. 28, 3303–3314.

Butler, M.H., David, C., Ochoa, G.C., Freyberg, Z., Daniell, L., Grabs, D., Cremona, O., De Camilli, P., 1997. Amphiphysin II (SH3P9; BIN1), a member of the Amphiphysin/Rvs family, is concentrated in the cortical cytomatrix of axon initial segments and nodes of ranvier in brain and around T tubules in skeletal muscle. J. Cell Biol. 137, 1355–1367.

Casal, E., Federici, L., Zhang, W., Fernandez-Recio, J., Priego, E.M., Miguel, R.N., DuHadaway, J.B., Prendergast, G.C., Luisi, B.F., Laue, E.D., 2006. The crystal structure of the BAR domain from human Bin1/Amphiphysin II and its implications for molecular recognition. Biochemistry 45, 12917–12928.

Davies, K.M., Anselmi, C., Wittig, I., Faraldo-Gómez, J.D., Kühlbrandt, W., 2012. Structure of the yeast F1Fo-ATP synthase dimer and its role in shaping the mitochondrial cristae. Proc. Natl. Acad. Sci. U.S.A. 109, 13602–13607.

Davies, K.M., Strauss, M., Daum, B., Kief, J.H., Osiewacz, H.D., Rycovska, A., Zickermann, V., Kühlbrandt, W., 2011. Macromolecular organization of ATP synthase and complex I in whole mitochondria. Proc. Natl. Acad. Sci. U.S.A. 108, 14121–14126.

Frangakis, A.S., Hegerl, R., 2001. Noise reduction in electron tomographic reconstructions using nonlinear anisotropic diffusion. J. Struct. Biol. 135, 239–250.

Hayashi, K., Miller, R.G., Brownell, K.W., 1987. Three-dimensional architecture of sarcoplasmic reticulum and T-system in human skeletal muscle. Anat. Rec. 218, 275–283.

Hilgemann, D.W., Feng, S., Nasuhoglu, C., 2001. The complex and intriguing lives of PIP2 with ion channels and transporters. Sci. STKE, re19.

Kerr, J.P., Ziman, A.P., Mueller, A.L., Muriel, J.M., Kleinhans-Welte, E., Gumerson, J.D., Vogel, S.S., Ward, C.W., Roche, J.A., Bloch, R.J., 2013. Dysferlin stabilizes stress-induced Ca^{2+} signaling in the transverse tubule membrane. Proc. Natl. Acad. Sci. U.S.A. 110, 20831–20836.

Kremer, J.R., Mastronarde, D.N., McIntosh, J.R., 1996. Computer visualization of three-dimensional image data using IMOD. J. Struct. Biol. 116, 71–76.

Lee, E., Marcucci, M., Daniell, L., Pypaert, M., Weisz, O.A., Ochoa, G.C., Farsad, K., Wenk, M.R., De Camilli, P., 2002. Amphiphysin 2 (Bin1) and T-tubule biogenesis in muscle. Science 297, 1193–1196.

Löw, C., Weininger, U., Lee, H., Schweimer, K., Neundorf, I., Beck-Sickinger, A.G., Pastor, R.W., Balbach, J., 2008. Structure and dynamics of helix-0 of the N-BAR domain in lipid micelles and bilayers. Biophys. J. 95, 4315–4323.

Matos, M.J., Post, J.A., Roelofsen, B., Op den Kamp, J.A.F., 1990. Composition and organization of sarcolemmal fatty acids in cultured neonatal rat cardiomyocytes. Cell Biol. Intern. Rep. 14, 343–352.

Mim, C., Unger, V.M., 2012. Membrane curvature and its generation by BAR proteins. Trends Biochem. Sci. 37, 526–533.

Mim, C., Cui, H., Gawronski-Salerno, J.A., Frost, A., Lyman, E., Voth, G.A., Unger, V.M., 2012. Structural basis of membrane bending by the N-BAR protein endophilin. Cell 149, 137–145.

Nicastro, D., 2009. Cryo-electron microscope tomography to study axonemal organization. Methods Cell Biol. 91, 1–39.

Ogata, T., Yamasaki, Y., 1997. Ultra-high-resolution scanning reticulum arrangement in human red, white, and intermediate muscle fibers. Anat. Rec. 248, 214–223.

Peter, B.J., Kent, H.M., Mills, I.G., Vallis, Y., Butler, P.J., Evans, P.R., McMahon, H.T., 2004. BAR domains as sensors of membrane curvature: the amphiphysin BAR structure. Science 303, 495–499.

Pettersen, E.F., Goddard, T.D., Huang, C.C., Couch, G.S., Greenblatt, D.M., Meng, E.C., Ferrin, T.E., 2004. UCSF Chimera – a visualization system for exploratory research and analysis. J. Comput. Chem. 25, 1605–1612.

Post, J.A., Langer, G.A., Op den Kamp, J.A.F., Verkleij, A.J., 1988. Phospholipid asymmetry in cardiac sarcolemma. Analysis of intact cells and 'gas-dissected' membranes. Biochim. Biophys. Acta 943, 256–266.

Post, J.A., Verkleij, A.J., Langer, G.A., 1995. Organisation and function of sarcolemmal phospholipids in control and ischemic/reperfused cardiomyocytes. J. Mol. Cell. Cardiol. 27, 749–760.

Razzaq, A., Robinson, I.M., McMahon, H.T., Skepper, J.N., Su, Y., Zelhof, A.C., Jackson, A.P., Gay, N.J., O'Kane, C.J., 2001. Amphiphysin is necessary for organization of the excitation-contraction coupling machinery of muscles, but not for synaptic vesicle endocytosis in *Drosophila*. Genes Dev. 15, 2967–2979.

Rosemblatt, M., Hidalgo, C., Vergara, C., Ikemoto, N., 1981. Immunological and biochemical properties of transverse tubule membranes isolated from rabbit skeletal muscle. J. Biol. Chem. 256, 8140–8148.

Shaikh, T.R., Gao, H., Baxter, W.T., Asturias, F.J., Boisset, N., Leith, A., Frank, J., 2008. SPIDER image processing for single-particle reconstruction of biological macromolecules from electron micrographs. Nat. Prot. 3, 1941–1974.

Suetsugu, S., Kurisu, S., Takenawa, T., 2014. Dynamic shaping of cellular membranes by phospholipids and membrane-deforming proteins. Physiol. Rev. 94, 1219–1248.

Van der Vusse, G.J., Van Bilsen, M., Reneman, R.S., 1994. Ischemia and reperfusion induced alterations in membrane phospholipids: an overview. Ann. N.Y. Acad. Sci. 723, 1–14.

Yoon, Y., Zhang, X., Cho, W., 2012. Phosphatidylinositol-4,5-bisphosphate (PtdIns (4,5)P$_2$) specifically induces membrane penetration and deformation by Bin/Amphiphysin/Rvs (BAR) domains. J. Biol. Chem. 287, 34078–34090.